

CHAPTER 3:

BARIUM TITANATE SPHERES AND SPHERICAL DISKS

3.1. INTRODUCTION

In the last chapter we discussed the two-beam coupling modules. In this chapter we discuss an idea with the original purpose of making two-beam coupling units even more compact: that of having a spherical barium-titanate crystal as the gain medium. Due to its curvature and high index of refraction, the lensing and gain effect of a photorefractive sphere can be combined to perform fiber-to-fiber two-beam coupling, dispensing the use of external lenses. The resulting two-beam coupling units with barium-titanate spheres are described in section 3.2 below.

We also found that, due to its high photorefractive gain, it is easy to excite whispering gallery modes (WGM) within the spherical crystal by shining a single pump beam onto it. Several patterns were observed, but the lowest order mode, the triangle pattern, was found to be the most robust. The WGM patterns can be better observed and documented when excited in a spherical disk, an equatorial slab of the sphere. In section 3.3 we discuss the oscillating patterns and compare the occurrence region of the triangle patterns with that predicted by a simple theoretical model.

3.2. PREPARATION

Optical quality spheres are straightforward to produce with hand lapping and polishing techniques. [Baxter,'50] We found that barium-titanate and lithium niobate are not substantially more difficult to form into a sphere than optical glass. The barium-titanate was electrically poled in its rectangular form before processing it into a sphere. We feared that barium titanate in particular might become depoled during processing, but such was not the case. Finished spheres of photorefractive barium titanate in fact turn out to be more robust to shocks than their delicate rectangular-cut counterparts, possibly due to the lack of sharp edges or corners from which cracks could propagate.

Spherical disks were produced by first forming a sandwich of two lithium-niobate slabs surrounding a slab of barium-titanate, held together by quartz wax. The sandwich is then lapped and polished into a sphere. Upon removing the lithium-niobate end-caps one is left with a barium-titanate disk with spherical sides, with the c-axis in the plane of the disk. Unlike the sphere, it is easy to observe through the flat top of the disk the beams as they propagate inside the crystal. We produced sphere and disk sizes from 3 mm to 7 mm diameter.

The c-axis of a 0° -cut photorefractive crystal is normally found by placing the crystal between two polarizers and identifying the widely-known conoscopic “iron cross”. The lensing property of the sphere morphs the iron cross into a “beach ball” as shown in Figure 3.1, thus it is easy to find and orient the c-axis of the sphere.

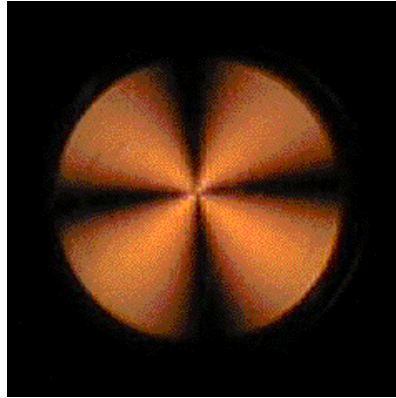


Figure 3.1. The “beach ball” pattern of a spherical photorefractive crystal between crossed polarizers observed directly along the c-axis.

3.3. TWO-BEAM COUPLING WITH SPHERES

Two-beam-coupling interaction can be made compact by taking advantage of the geometry of the spheres and the high index of refraction of barium titanate, which is greater than 2 throughout the visible spectrum. Due to these properties, the crystal can directly image the light from one optical fiber to another. In a symmetrical arrangement, the collimated beam inside the sphere can be photorefractively coupled to a second beam propagating between a second pair of fibers. Figure 3.2 shows direct fiber-to-fiber two-beam coupling using a photorefractive sphere without other intervening optical elements. The sphere conveniently magnifies the interaction region viewed by the camera. Two beams, at 514 nm wavelength, cross inside the crystal and undergo two-beam coupling. Each beam is associated with a pair of multimode gradient index fibers, with a 62.5 μm core diameter. With a spherical disk

of 4 mm diameter, the collimated size of the laser beam in the crystal is about 0.8 mm when the fiber-to-fiber imaging is optimized. The apparatus allowed rotation of the crystal axis continuously and permitted the angle between the beams to be chosen from 5° to 45° in 5° increments. Maximum gain occurred at the expected 45° between the c-axis and input beam bisector. The optimum beam angle was observed to be $10^\circ \pm 2.5^\circ$ - larger than the 4° - 6° typically estimated in theoretical plane-wave calculations. [Fainman,'86] Gain was measured using a loss-to-gain beam ratio of $10^5:1$ and a gain-beam strength of $0.5 \mu\text{W}$. As in the previous chapter, we define gain to be the ratio of the gain-beam intensity at the output of its fiber with the loss-beam present to its intensity with the loss-beam blocked. Because the light from the fibers is unpolarized, one expects an effective reduction of the coupling constant by a factor of 2. We nevertheless obtained a maximum gain of 8000, which is comparable to gains obtained with rectangular-cut crystals of similar length.¹

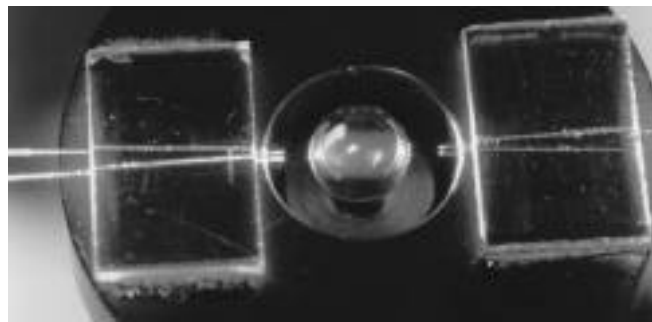


Figure 3.2. Two-beam coupling between two pairs of fibers using a spherical photorefractive crystal of barium titanate.

¹ The two-beam coupling unit was built and tested by Edeline Fotheringham.

3.4. WHISPERING-GALLERY MODE PATTERNS

We have also investigated interesting oscillation patterns that occur when a Gaussian (free-space) pump is incident on the spherical disk. The oscillating patterns are understood to be low-order whispering gallery modes which are generated by total internal reflection at the crystal's boundaries.

The modes of a spherical resonator that propagate by total-internal reflection at the surface were first analyzed by Lord Rayleigh for acoustic waves and he referred to the analysis as "The problem of the whispering gallery". [Lindsay,'70] Baer demonstrated continuous-wave active excitation of whispering gallery modes using a Nd:YAG sphere pumped with a diode laser. [Baer,'87] Demonstration of active oscillation of whispering gallery modes in a gamut of other materials (and structures) followed, such as in fused-silica [Schiller,'91], polymers [Kuwata-Gonokami,'95], semiconductors [Courtney,'98], and organic materials [Lin,'98]. In these demonstrations oscillation arises from stimulated emission, whereas in our photorefractive spheres oscillation arises from two-beam-coupling, a parametric interaction between the incident pump, the loss beam, and the modes of the resonator, the gain beams.

3.4.1. A family of patterns

At a wavelength of 532 nm, the critical angle for total internal reflection is $\arcsin(1/2.4)$, about 25° , thus the lowest order whispering gallery mode of a barium-titanate sphere or disk is a triangle. Since the maximum two-beam coupling gain for barium titanate occurs for small loss-to-gain interbeam angles, one expects the patterns to orient themselves such as to minimize this angle. As shown in figure 3.3 for the triangle and square, the interbeam angle is minimum when a vertex of the pattern aligns itself with either the incident pump location or with the pump's first reflection location. (Second and higher pump reflections are too weak to excite patterns.) We call the former "front-side" patterns (shown with full lines in figure 3.3) and the latter "back-side" patterns (shown with dashed lines). As also shown in figure 3.3, the minimum possible interbeam angle occurs for maximum displacement of the pump, giving 5° for a triangle, 20° for a square and larger for higher-order regular polygons. Since this interbeam angle is smaller for lower order patterns, and smaller interbeam angle translates into higher gain, we expect the triangle to be both the strongest oscillating mode and the easiest to excite.

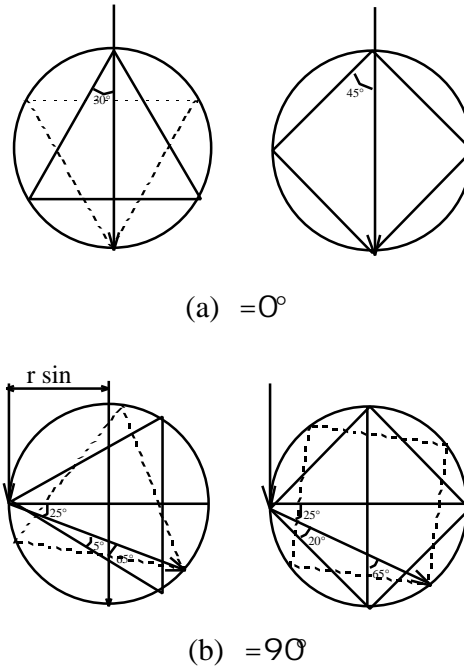


Figure 3.3. Diagrams of minimum interbeam angles. (a) Pump propagates directly down the center of the crystal. (b) Pump is incident at maximum displacement ($r \sin$) from center. In every case, the minimum interbeam angle occurs when vertices are aligned with the pump incidence location (full line triangle and square) or when vertices are aligned with pump's first reflection location (dashed line).

Our experiments reveal that this is indeed the case. The setup used for observing the oscillating patterns is shown in figure 3.4, and pictures of the patterns in figure 3.5. Figure 3.5 (a) shows a front-side oscillating triangle mode in a 5.2 mm diameter spherical disk. In the figure, the pump beam enters the crystal in the vertically downward direction. The pump beam is focused by a microscope objective so that a beam waist occurs inside the disk and is roughly matched in position with a waist of the mode. Most of the pump energy is depleted in the first millimeter after the pump enters the disk, indicating efficient energy transfer. Back-side oscillation

also occurs when the crystal c-axis is appropriately rotated. In Figure 3.5 (b) gain is provided to the triangle by the reflection of the pump off of the far-side surface. In this instance the microscope objective is adjusted to collimate the beam in the disk. The oscillation is weaker than the front-side case since the pump intensity is reduced by both absorption and transmission (causing the pump to exit the crystal).

Other modes are excited by changing the orientation of the c-axis, the lateral position of the pump, as well as the pump's angular distribution. Figures 3.5 (c) and (d) show a front-side and back-side square respectively. As explained above, they are much weaker than the triangle because the two-beam coupling gain falls off rapidly with pump-signal angle. We have observed squares in isolation but they were too weak to photograph well. Many patterns can be excited simultaneously under certain conditions. Close inspection of Figure 3.5 (e) reveals a triangle, a square, and a pentagon. For higher angular distribution of the pump, the triangles tend to get blurred, i.e., they also acquire a high angular distribution, as shown in figures 3.5 (c) and (f). Higher order modes are weaker and tend to be difficult to observe both because they experience less gain as the order grows and because they are obscured by the spherical curvature of the disk outer surface. Hexagons were the highest order observed and multiple patterns such as David stars (two interlaced triangles) were also observed.

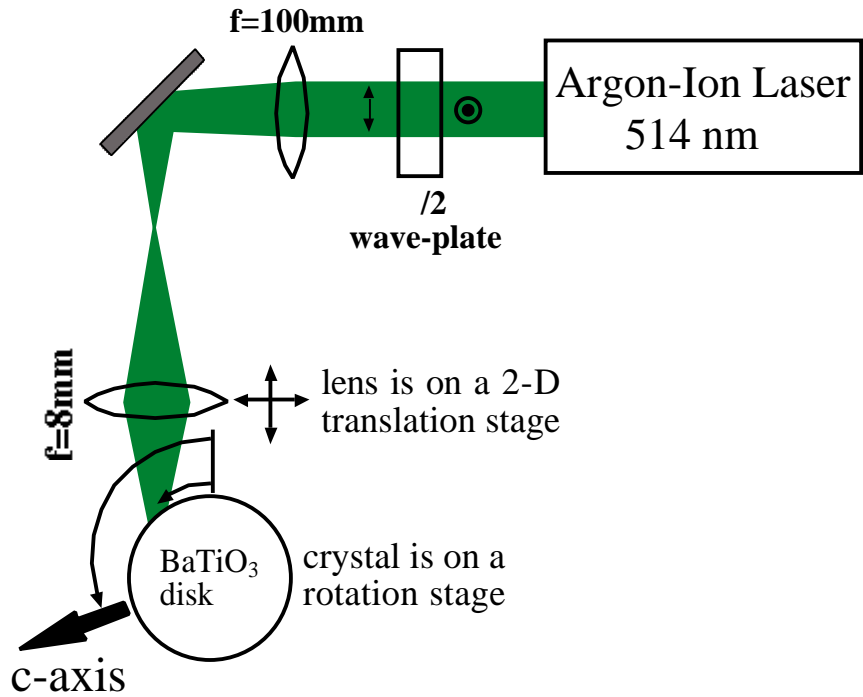


Figure 3.4. Experimental setup for observing oscillating patterns. The angular displacement of the pump is given by θ and the rotation of the c-axis by ϕ . Note that the parameters θ and ϕ are measured with respect to the vertical line (parallel to the pump) which crosses the center of the crystal.

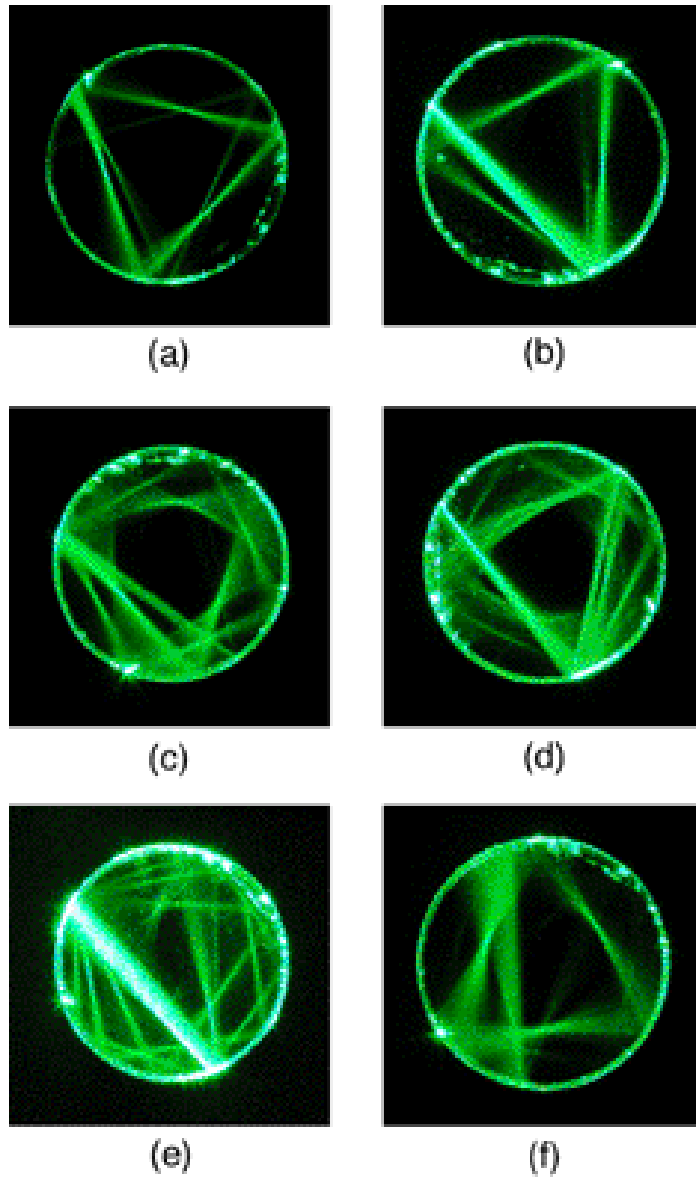


Figure 3.5. Oscillation patterns inside a barium titanate spherical disk.

3.4.2. A theory for the triangle occurrence regions

As further investigation we calculate the gain maxima for triangle excitation using a simple model which uses two-beam coupling of the pump with one side of the triangle. The calculations assume plane-waves for the interacting beams. Specifically, we calculate the c-axis orientation which maximizes the gain for the triangle as a function of the incoming pump-beam angle. Figures 3.6 (a) and (b) show the geometrical relations used in our calculations for a front-side and a back-side triangle respectively. For an input displacement of the pump, given by $r \sin(\theta)$, the minimum interbeam angle is given by $2\theta = 3\theta_c$, where θ_c is the refraction angle with respect to the surface's normal. The two-beam coupling gain curve, given by the expression (see chapter 1, section 1.2)

$$\gamma = \frac{2\pi}{n\lambda \cos\theta} r_{eff}, \quad \text{where } r_{eff} = -2 n_o^2 n_e^2 r_{42} E_{sc}(\theta, \varphi) \cos\alpha \sin(2\varphi), \quad [3.1]$$

has two maxima when plotted as a function of the c-axis orientation θ for a fixed interbeam half-angle θ . Therefore, for each value of the interbeam angle 2θ above we can find from the gain curve two c-axis orientations, θ_d and θ_r , corresponding to the two maxima. The angles θ_d and θ_r give the direction of the crystal axis with respect to the bisector of the two interacting beams. The subscript in θ_d stands for “direct” denoting that the c-axis direction is less than 90° apart from the bisector, whereas θ_r stands for “reverse”, and has a value between 90° and 180° . To compare our results to

the measurements, we must reference the direct and reverse c-axis angles to the direction of the incoming pump (the vertical in figure 3.6) thereby obtaining θ_d and θ_r . Taking both front-side and back-side configurations in figure 3.6 into account, we end up with four optimum c-axis orientations, yielding four theoretical curves of η as a function of the input pump-beam angle θ .

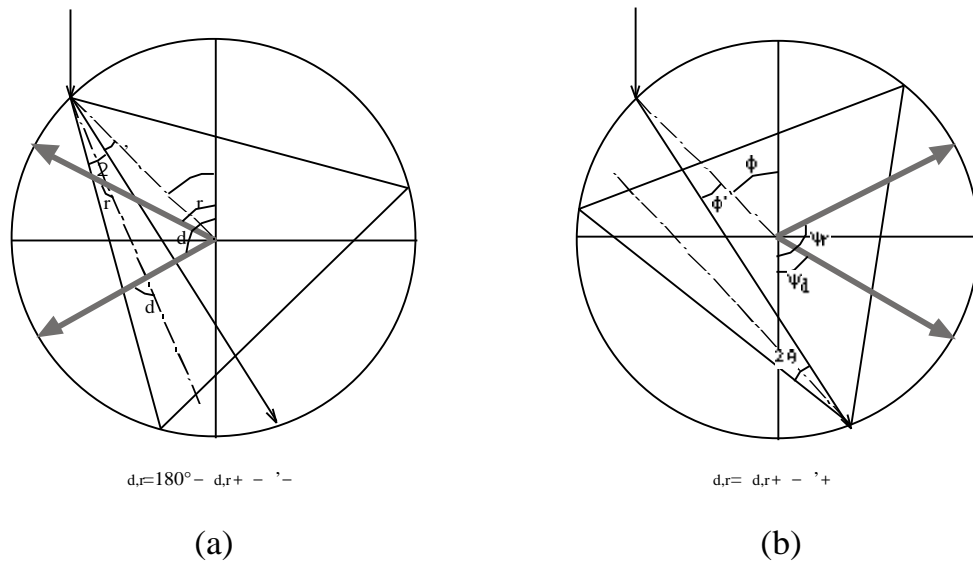


Figure 3.6. Schematic showing the geometrical relationship between θ and θ_r for a (a) front-side and (b) back-side triangle. For a given θ , there are two optimum values of θ_r that maximizes the two-beam coupling gain, resulting in also two optimum values of θ_d , namely θ_{d+} and θ_{d-} .

Figure 3.7 shows the occurrence map for triangles with respect to the incident pump-beam angle (θ) and the orientation of the crystal axis (θ_d). Both angles are

referenced to the line that crosses the center of the disk and is parallel to the external incident pump. The four above-mentioned calculated curves (thin lines), corresponding to the theoretical gain maxima, are superimposed over the measured triangle regions (thick horizontal lines). The triangle structures occur over a wide variety of beam parameters. Figure 3.7 shows a reasonable qualitative agreement between the measured regions and the maximum gain calculations. The superposed dotted-lined ellipses are meant to qualitatively indicate the range of parameters over which triangles are observed.

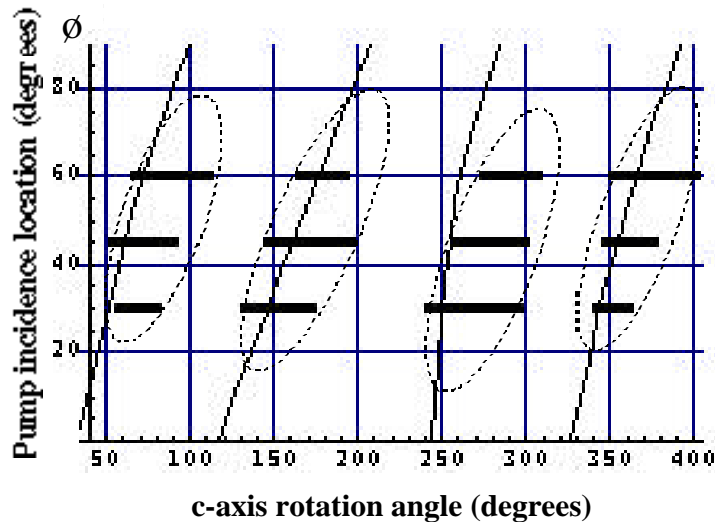


Figure 3.7. Triangle occurrence regions. Dotted ellipses qualitatively show the four regions of the parameter space for which triangles are observed (the pump beam size and divergence are fixed). The horizontal bars show quantitative data regions of triangles. The solid lines represent the four theoretical curves of () that maximize gain. (The parameter-space coordinates are defined in either figure 3.4 or 3.6.)

3.4.3. Unidirectional oscillation

Two qualitative observations suggest that the oscillating patterns are unidirectional and in the forward direction defined by the pump. First, we observe that the light scattered from nonuniformities in the crystal to be in the forward direction. Second, we never observed a steady phase-conjugate beam. In rectangular-cut crystals self-pumped phase-conjugation of a single pump beam is often observed. [Feinberg,'82] The corners of the crystals act as corner-reflectors that generates the phase-conjugated beam via four-wave mixing. Since the disks and spheres have no corners one might wonder whether self-pumped phase-conjugation can occur. In fact, we were never able to observe steady-state phase-conjugation of the input pump-beam under *any* circumstances in any of our sphere or disk samples. We were able to observe highly unsteady phase-conjugation of the pump beam at normal incidence to the crystal, along the c-axis direction.¹

3.5. CONCLUSIONS

The spherical barium titanate crystal is interesting for several reasons. Most systems built in our laboratories employ two-beam coupling as a basic function. In many cases, the two-beam coupling unit is used to pump a ring oscillator, such as the case of the auto-tuning filter, which we discussed in the previous chapter and will

¹ Phase-conjugation observations were done by Dr. Dana Anderson and Dr. Vladimir Shkunov.

revisit in the next chapter. By allowing fiber-to-fiber two-beam coupling, the spheres contribute in building compact systems. Compactness not only has the advantage of making photorefractive systems portable and light weight, but also of reducing vibrations and increasing robustness, this last due to the decreased number of elements necessary in the system. The WGM patterns, for now, are only a scientific curiosity. However, one can think of them as a very compact ring oscillator inside the crystal itself. To make them useful for real systems one needs find a practical way of coupling some of the oscillation light out of the crystal. That could be done by frustrating one of the reflections of the oscillating pattern [Schiller, '92] and then coupling to an optical fiber.

Finally, the spherical disk geometry with the c-axis in the plane of the disk is convenient for determining two-beam coupling parameters. In particular, the internal beam angles are not restricted as they are in rectangular-cut samples by Snell's law and the beam geometry is practically independent of crystal orientation, though there is some degree of optical asphericity due to crystal birefringence.